



PAPER

Probabilistic RNA Designability via Interpretable Ensemble Approximation and Dynamic Decomposition

Tianshuo Zhou¹ David H. Mathews^{3,4,5} and Liang Huang^{1,2,*}

¹School of EECS, ²Dept. of Biochemistry & Biophysics, Oregon State University, USA, ³Dept. of Biochemistry & Biophysics, ⁴Center for RNA Biology and ⁵Dept. of Biostatistics and Computational Biology, University of Rochester Medical Center, USA

*Corresponding author. liang.huang.sh@gmail.com

FOR PUBLISHER ONLY Received on Date Month Year; revised on Date Month Year; accepted on Date Month Year

Abstract

Motivation: RNA design aims to find RNA sequences that fold into a given target secondary structure, a problem also known as RNA inverse folding. However, not all target structures are designable. Recent advances in RNA designability have focused primarily on *minimum free energy* (MFE)-based criteria, while *ensemble*-based notions of designability remain largely underexplored. To address this gap, we introduce a theory of ensemble approximation and a probability decomposition framework for bounding the folding probabilities of RNA structures in an explainable way. We further develop a linear-time dynamic programming algorithm that efficiently searches over exponentially many decompositions and identifies the optimal one that yields the tightest probabilistic bound for a given structure.

Results: Applying our methods to both native and artificial RNA structures in the ArchiveII and Eterna100 benchmarks, we obtained probability bounds that are much tighter than prior approaches. In addition, our methods further provide anatomical tools for analyzing RNA structures and understanding the sources of design difficulty at the motif level.

Availability: Source code and data are available at <https://github.com/shanry/RNA-Undesign>.

Supplementary information: Supplementary text and data are available in a separate PDF.

Contact: liang.huang.sh@gmail.com

Key words: RNA Design, RNA Designability, RNA Inverse Folding, Equilibrium Probability

1. Introduction

RNA secondary structures play crucial roles in the functions of non-coding RNAs such as rRNA (Doudna and Cech, 2002) and tRNA (Coller and Ignatova, 2024). RNA design (Portela, 2018; Zhou *et al.*, 2023), also known as RNA inverse folding, aims to find one or more RNA sequences that fold into a given target structure, typically using the default Turner energy model (Mathews and Turner, 2006; Turner and Mathews, 2010). However, not all RNA structures are designable (Aguirre-Hernández *et al.*, 2007; Yao, 2021; Zhou *et al.*, 2024, 2025) under the Turner energy model. The recent works RIGEND (Zhou *et al.*, 2024) and FastMotif (Zhou *et al.*, 2025) proved that many native structures in the benchmark ArchiveII and many artificial structures in the benchmark Eterna100 are undesignable. However, both methods focus exclusively on MFE-based criteria and therefore provide only a binary notion of designability. As a result, they cannot address

ensemble-level design objectives such as equilibrium probability.

Recent studies (Ward *et al.*, 2023) suggest that equilibrium probability is a more appropriate optimization objective for RNA design than structural distance or ensemble defect. This perspective motivates a shift from binary MFE-based criteria to a probabilistic characterization of designability under the Turner energy model. While MFE-based undesignability can certify that a structure is impossible to be a minimum free energy structure of any RNA sequence, it cannot quantify *how likely* or the maximum folding probability that a structure is able to form in Boltzmann ensembles. For example, consider two structures \mathbf{y}_1 and \mathbf{y}_2 that are both undesignable under the MFE or unique MFE (uMFE) criterion. It is nevertheless possible that there exists a sequence \mathbf{x} for which the probability $p(\mathbf{y}_1 \mid \mathbf{x})$ reaches 0.2, whereas no sequence can make $p(\mathbf{y}_2 \mid \mathbf{x})$ exceed 0.01.

This discrepancy is invisible to MFE-based analysis but is crucial for understanding practical designability and RNA folding models. These observations motivate the study of *probabilistic designability*, defined as an upper bound on $p(\mathbf{y}^* | \mathbf{x})$ for a given target structure \mathbf{y}^* . The tighter the upper bound, the better we understand the thermodynamics of RNA folding.

Despite its importance, probabilistic designability has received little attention in RNA design. To the best of our knowledge, CountingDesign (Yao et al., 2019; Yao, 2021) is the main existing method that addresses this question. However, it relies on exhaustive enumeration: for a given RNA structure or structural motif, it enumerates all (partial) sequences that satisfy its base-pairing constraints, fold each sequence, and record the maximum equilibrium probability observed. This brute-force strategy is neither scalable nor interpretable, requiring weeks of computation for structures or motifs of length up to 14.

To bridge the gap between MFE-based and probabilistic designability, we propose two theories: *ensemble approximation* and *probability decomposition*. Ensemble approximation represents the full RNA folding ensemble using a small, explicitly identified set of rival structures (motifs) that compete with the target structure. This approximated ensemble enables us to derive rigorous upper bounds on folding probability while maintaining full explainability, as each bound is supported by concrete rival structures that thermodynamically dominate the target. Furthermore, we establish that the probability bound of a target structure is no greater than the *product of the local probability bounds* of its constituent motifs under any structural decomposition. Leveraging this property, we develop a linear-time dynamic programming algorithm that efficiently considers exponentially many decompositions and selects the one yielding the tightest upper bound. Our contributions are:

1. **Theory.** We propose a novel and elegant theory of ensemble approximation to interpretably characterize probabilistic RNA designability. We prove that the probability bound of a structure can be decomposed into local bounds of structural motifs, revealing a more nuanced connection between local and global designability.
2. **Algorithms.** We develop efficient algorithms for approximating Boltzmann ensembles using rival structures or motifs, and introduce a linear-time dynamic programming approach that efficiently explores exponentially many decompositions to obtain a probability bound as tight as possible.
3. **Application.** Applying our methods to both native and artificial RNA structures in the ArchiveII and Eterna100 benchmarks, we obtained probability bounds that are much tighter than prior approaches. In addition, our methods further provide anatomical tools for analyzing RNA structures and understanding the sources of design difficulty at the motif level.

2. Probabilistic RNA Designability

2.1. RNA Structure and Free Energy

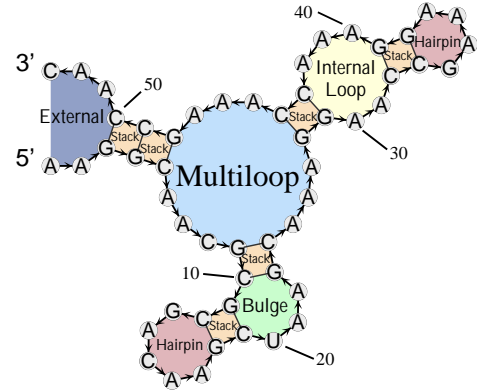


Fig. 1. An example of secondary structure and its loops.

An RNA sequence \mathbf{x} of length n is specified as a string of base nucleotides $\mathbf{x}_1 \mathbf{x}_2 \dots \mathbf{x}_n$, where $\mathbf{x}_i \in \{A, C, G, U\}$ for $i = 1, 2, \dots, n$. The length of \mathbf{x} can also be denoted as $|\mathbf{x}|$. A secondary structure \mathcal{P} for \mathbf{x} is a set of paired indices where each pair $(i, j) \in \mathcal{P}$ indicates two distinct bases $\mathbf{x}_i \mathbf{x}_j \in \{CG, GC, AU, UA, GU, UG\}$ and each index from 1 to n can only be paired once. A secondary structure is pseudoknot-free if there are no two pairs $(i, j) \in \mathcal{P}$ and $(k, l) \in \mathcal{P}$ such that $i < k < j < l$. In short, a pseudoknot-free secondary structure is a properly nested set of pairings in an RNA sequence. Alternatively, \mathcal{P} can be represented as a string $\mathbf{y} = \mathbf{y}_1 \mathbf{y}_2 \dots \mathbf{y}_n$, where a pair of indices $(i, j) \in \mathcal{P}$ corresponds to $\mathbf{y}_i = "(", \mathbf{y}_j = ")"$ and any unpaired index k corresponds to $\mathbf{y}_k = "."$. The unpaired indices in \mathbf{y} are denoted as *unpaired*(\mathbf{y}) and the set of paired indices in \mathbf{y} is denoted as *pairs*(\mathbf{y}), which is equal to \mathcal{P} . Here we do not consider pseudoknots.

The *ensemble* of an RNA sequence \mathbf{x} is the set of all secondary structures that \mathbf{x} can possibly fold into, denoted as $\mathcal{Y}(\mathbf{x})$. The *free energy (change)* $\Delta G^\circ(\mathbf{x}, \mathbf{y})$ is used to characterize the stability of $\mathbf{y} \in \mathcal{Y}(\mathbf{x})$. The lower the free energy change, $\Delta G^\circ(\mathbf{x}, \mathbf{y})$, the more stable the secondary structure \mathbf{y} for \mathbf{x} .

A structure \mathbf{y} is composed of a set of loops denoted as *loops*(\mathbf{y}), as illustrated in Fig. 1. The free energy change of a secondary structure \mathbf{y} is the sum of the free energy change of each loop, i.e.,

$$\Delta G^\circ(\mathbf{x}, \mathbf{y}) = \sum_{\mathbf{z} \in \text{loops}(\mathbf{y})} \Delta G^\circ(\mathbf{x}, \mathbf{z}), \quad (1)$$

where each term $\Delta G^\circ(\mathbf{x}, \mathbf{z})$ is the energy for loop \mathbf{z} . The energy of each loop is typically determined by nucleotides on the positions of enclosing pairs and their adjacent mismatch positions, which are named as *critical positions* and denoted as *critical*(\mathbf{z}). See Supplementary Section S1 for a detailed explanation of different loop types and their critical positions. The structure with the *minimum free energy* is the most stable structure in the ensemble $\mathcal{Y}(\mathbf{x})$.

The minimum free energy of $\mathcal{Y}(\mathbf{x})$ is denoted as $\text{MFE}(\mathbf{x})$ and defined as

$$\text{MFE}(\mathbf{x}) = \min_{\mathbf{y} \in \mathcal{Y}(\mathbf{x})} \Delta G^\circ(\mathbf{x}, \mathbf{y}). \quad (2)$$

The equilibrium probability or folding probability of a structure \mathbf{y} in the ensemble of \mathbf{x} is defined based on the partition function, $Q(\mathbf{x})$,

$$p(\mathbf{y} \mid \mathbf{x}) = \frac{e^{-\Delta G^\circ(\mathbf{x}, \mathbf{y})/RT}}{Q(\mathbf{x})} = \frac{e^{-\Delta G^\circ(\mathbf{x}, \mathbf{y})/RT}}{\sum_{\mathbf{y}' \in \mathcal{Y}(\mathbf{x})} e^{-\Delta G^\circ(\mathbf{x}, \mathbf{y}')/RT}}. \quad (3)$$

A (structural) *motif* is defined as a contiguous set of loops in a structure, which makes motifs can be considered as a generalization of RNA structure (See Supplementary Section S2 or FastMotif (Zhou *et al.*, 2024) for details). The thermodynamic definitions in Eqs. (1) to (3) can be naturally extended to motifs. For example, the equilibrium probability of a motif \mathbf{m} in the ensemble of \mathbf{x} is

$$p(\mathbf{m} \mid \mathbf{x}) = \frac{e^{-\Delta G^\circ(\mathbf{x}, \mathbf{m})/RT}}{Q(\mathbf{x})} = \frac{e^{-\Delta G^\circ(\mathbf{x}, \mathbf{m})/RT}}{\sum_{\mathbf{m}' \in \mathcal{M}(\mathbf{x})} e^{-\Delta G^\circ(\mathbf{x}, \mathbf{m}')/RT}}, \quad (4)$$

where $\mathcal{M}(\mathbf{x})$ is the motif ensemble of the (parital) sequence \mathbf{x} .

2.2. MFE-based Designability

Given a target structure \mathbf{y}^* , MFE-based RNA design aims to find a suitable RNA sequence \mathbf{x} such that \mathbf{y}^* is an MFE structure of \mathbf{x} . For convenience, we define $\mathcal{X}(\mathbf{y})$ as the set of all RNA sequences whose ensemble contains \mathbf{y} , i.e., $\mathcal{X}(\mathbf{y}) = \{\mathbf{x} \mid \mathbf{y} \in \mathcal{Y}(\mathbf{x})\}$. a structure \mathbf{y}^* is undesignable by the MFE criterion if and only if

$$\forall \mathbf{x} \in \mathcal{X}(\mathbf{y}), \exists \mathbf{y}' \neq \mathbf{y}^*, \Delta G^\circ(\mathbf{x}, \mathbf{y}') < \Delta G^\circ(\mathbf{x}, \mathbf{y}), \quad (5)$$

where $\mathcal{X}(\mathbf{y})$ denotes all the RNA sequences satisfying the base pair constraints of \mathbf{y}^* .

Following the unique MFE (uMFE) criterion from previous studies (Haleš *et al.*, 2015; Yao *et al.*, 2019; Ward *et al.*, 2023; Zhou *et al.*, 2023), a structure \mathbf{y}^* is undesignable by the (uMFE) criterion if and only if

$$\forall \mathbf{x} \in \mathcal{X}(\mathbf{y}), \exists \mathbf{y}' \neq \mathbf{y}^*, \Delta G^\circ(\mathbf{x}, \mathbf{y}') \leq \Delta G^\circ(\mathbf{x}, \mathbf{y}). \quad (6)$$

2.3. Probabilistic Designability

MFE-based designability cannot quantify *how likely* a target structure can possibly form in the ensemble of any RNA sequence. To address this problem, we aim to find an upper bound $p_{\text{bound}}(\mathbf{y})$ such that $\max_{\mathbf{x}} p(\mathbf{y} \mid \mathbf{x}) \leq p_{\text{bound}}(\mathbf{y})$. While it is hard to obtain the exact value of $\max_{\mathbf{x}} p(\mathbf{y} \mid \mathbf{x})$, the tighter $p_{\text{bound}}(\mathbf{y})$ is, the better we know about the probabilistic designability of \mathbf{y} . Similarly, we can also find an upper bound $p_{\text{bound}}(\mathbf{m})$ for a motif \mathbf{m} such that $\max_{\mathbf{x}} p(\mathbf{m} \mid \mathbf{x}) \leq p_{\text{bound}}(\mathbf{m})$.

3. Ensemble Approximation via Rival Search

Rival structures (motifs) play a pivotal role in the previous works RIGEND (Zhou *et al.*, 2024) and FastMotif (Zhou

et al., 2025), which can prove RNA structures (motifs) undesignable under the uMFE criterion. The central idea is to identify a small set of rival structures (motifs)

$$Y_r = \{\mathbf{y}_1, \mathbf{y}_2, \dots, \mathbf{y}_k\}, \mathbf{y}^* \notin Y_r,$$

such that

$$\forall \mathbf{x}, \exists \mathbf{y}' \in Y_r, \Delta G^\circ(\mathbf{x}, \mathbf{y}') \leq \Delta G^\circ(\mathbf{x}, \mathbf{y}^*). \quad (7)$$

In other words, for every RNA sequence \mathbf{x} , at least one explicitly identified rival structure is energetically no worse than the target structure. This condition guarantees that the target structure can never be the unique minimum free energy conformation of any sequence and is therefore uMFE-undesignable.

While effective, both RIGEND and FastMotif treat rival structures as *independent* competitors. Consequently, the collective thermodynamic effect of multiple rival structures is left unexploited. In this section, we introduce a new theory of Boltzmann ensemble approximation that leverages the collective contribution of rival structures to derive an upper bound on the equilibrium probability of the target structure.

To make the derivation intuitive, we begin with the simplest case, in which the ensemble is approximated by the target structure and a single rival structure. We then extend this theory to the general case, where the ensemble approximation consists of multiple rival structures (motifs). Since motifs are generalizations of structures, we present the theory using structures for notational simplicity; all results apply to motifs directly.

3.1. Ensemble Approximation with a Single Rival Structure (Motif)

We illustrate the idea using the Eterna100 structure “Simple Single Bond” (by cutting off some trailing unpaired bases to fit the page). When attempting to design this target structure \mathbf{y}^* (Fig. 2), the resulting sequence \mathbf{x} consistently folds into a different but structurally very similar conformation \mathbf{y}' .

\mathbf{y}^* :(.....(((.....)))).....
 \mathbf{y}' :((.....(((.....)))).....
 \mathbf{x} : AUAAGCGGUAAAAAGUGCGAAAAGCAUGAAAAAAACAGA
 Δ : *** ** * ***

Fig. 2. Ensemble approximation with a single rival structure.

As proven in RIGEND (Zhou *et al.*, 2024), it turns out that the free energy change difference

$$\Delta \Delta G^\circ(\mathbf{x}, \mathbf{y}', \mathbf{y}^*) \triangleq \Delta G^\circ(\mathbf{x}, \mathbf{y}') - \Delta G^\circ(\mathbf{x}, \mathbf{y}^*)$$

between \mathbf{y}' and \mathbf{y}^* is only dependent on a few *differential positions*

$$\Delta(\mathbf{y}', \mathbf{y}^*) \triangleq \bigcup_{\mathbf{z} \in \text{loops}(\mathbf{y}^*) \ominus \text{loops}(\mathbf{y}')} \text{critical}(\mathbf{z}).$$

Fig. 2 annotates the differential positions at the last line. Consequently, to verify that $\Delta \Delta G^\circ(\mathbf{x}, \mathbf{y}', \mathbf{y}^*) <$

0 holds for all sequences \mathbf{x} , it suffices to enumerate nucleotide assignments restricted to $\Delta(\mathbf{y}', \mathbf{y}^*)$. This reduction enables an efficient and interpretable proof that \mathbf{y}^* is undesignable under the uMFE criterion. Beyond the uMFE undesignability, however, we notice that this process yields additional thermodynamic insight. In particular, rather than merely establishing the sign of $\Delta\Delta G^\circ(\mathbf{y}', \mathbf{y}^*)$, we can compute the quantity,

$$\max_{\mathbf{x}} \Delta\Delta G^\circ(\mathbf{x}, \mathbf{y}', \mathbf{y}^*),$$

which represents the guaranteed energy advantage of the rival structure over the target across all sequences. This quantity directly leads to an upper bound on the equilibrium probability of the target structure. Specifically,

$$\begin{aligned}
p(\mathbf{y}^* \mid \mathbf{x}) &= \frac{e^{-\Delta G^\circ(\mathbf{x}, \mathbf{y}^*)/RT}}{\sum_{\mathbf{y} \in \mathcal{Y}(\mathbf{x})} e^{-\Delta G^\circ(\mathbf{x}, \mathbf{y})/RT}} \\
&\leq \frac{e^{-\Delta G^\circ(\mathbf{x}, \mathbf{y}^*)/RT}}{e^{-\Delta G^\circ(\mathbf{x}, \mathbf{y}^*)/RT} + e^{-\Delta G^\circ(\mathbf{x}, \mathbf{y}')/RT}} \\
&= \frac{1}{1 + e^{-(\Delta G^\circ(\mathbf{x}, \mathbf{y}') - \Delta G^\circ(\mathbf{x}, \mathbf{y}^*))/RT}}. \tag{8}
\end{aligned}$$

Taking the maximum over all sequences \boldsymbol{x} , we obtain the following upper bound:

$$\max_{\mathbf{x}} p(\mathbf{y}^* \mid \mathbf{x}) \leq \frac{1}{1 + e^{-(\max_{\mathbf{x}} \Delta \Delta G^\circ(\mathbf{x}, \mathbf{y}', \mathbf{y}^*))/RT}}. \quad (9)$$

The Algorithm 1 shows the specific steps to identify an upper bound for $\max_{\mathbf{x}} p(\mathbf{y}^* \mid \mathbf{x})$ using a single rival structure.

Algorithm 1 Ensemble Approximation with a Single Rival Structure (Motif)

```

function ENSEMBLEAPPROXIMATION( $y^*$ ,  $y'$ )
   $\Delta\Delta G_{max}^o \leftarrow -\infty$ 
  for  $\hat{x} \in \{x \vdash \Delta(y', y^*) \mid x \in \mathcal{X}(y^*)\}$  do
    if  $\Delta\Delta G^o(\hat{x}, y', y^*) > \Delta\Delta G_{max}^o$  then
       $\Delta\Delta G_{max}^o = \Delta\Delta G^o(\hat{x}, y', y^*)$ 
  return  $\frac{1}{1 + e^{-\Delta\Delta G_{max}^o / RT}}$      $\triangleright$  upper bound  $pbound(y^*)$ 

```

3.2. Ensemble Approximation with Multiple Rival Structures (Motifs)

Although Algorithm 1 is effective and interpretable, the resulting bound is limited by the coarse approximation of the ensemble using only one rival structure. In principle, incorporating more rival structures yields a tighter approximation, though enumerating the full ensemble is infeasible.

We therefore generalize the framework to include multiple rival structures. Figure 3 illustrates this idea using the Eterna100 structure ‘‘Zigzag Semicircle’’. Our previous work (Zhou *et al.*, 2024) proved this structure uMFE-undesignable by identifying a set of nine rival

```

 $y^*:$  ....((((((.((....)).).).))).))....  

 $y^{*1}:$  ....((((((..((....)).).).))).))....  

 $y^{*2}:$  ....((((((.((....)).)).).))).))....  

 $y^{*3}:$  ....(((((((((....)).)).).))).))....  

 $y^{*4}:$  ....((((((.((....)).).).))).))....  

 $y^{*5}:$  ....((((((.(((....)).).).))).))....  

 $y^{*6}:$  ....(((((((((....)).).).))).))....  

 $y^{*7}:$  ....((((((.(((....)).)).).))).))....  

 $y^{*8}:$  ....((((((..((....)).).).))).))....  

 $y^{*9}:$  ....((((((.....))).))).))....  

^

```

Fig. 3. Example of ensemble approximation with multiple rival structures

structures

$$\forall x, \exists y' \in Y_r = \{y'^1, y'^2, \dots, y'^9\},$$

such that

$$\Delta\Delta G^\circ(x, y', y^*) \leq 0.$$

Rather than selecting a single rival, we include all nine rivals in the ensemble approximation to obtain a tighter bound. Specifically,

$$\begin{aligned}
p(\mathbf{y}^* \mid \mathbf{x}) &\leq \frac{e^{-\Delta G(\mathbf{x}, \mathbf{y}^*)/RT}}{e^{-\Delta G(\mathbf{x}, \mathbf{y}^*)/RT} + \sum_{\mathbf{y}' \in Y_r} e^{-\Delta G(\mathbf{x}, \mathbf{y}')/RT}} \\
&\leq \frac{1}{1 + \sum_{\mathbf{y}' \in Y_r} e^{-(\Delta G(\mathbf{x}, \mathbf{y}') - \Delta G(\mathbf{x}, \mathbf{y}^*))/RT}} \quad (10) \\
&\leq \frac{1}{1 + \sum_{\mathbf{y}' \in Y_r} e^{-(\Delta \Delta G^{\circ}(\mathbf{x}, \mathbf{y}', \mathbf{y}^*))/RT}} \\
&\leq \frac{1}{1 + e^{-(\Delta \Delta G^{\circ}(\mathbf{x}, Y_r, \mathbf{y}^*))/RT}},
\end{aligned}$$

where $e^{-(\Delta\Delta G^\circ(\mathbf{x}, Y_r, \mathbf{y}^*))/RT}$ summarizes the collective energetic dominance of the rival set over the target structure. Taking the maximum over all sequences yields

$$\max_{\mathbf{x}} p(\mathbf{y}^* \mid \mathbf{x}) \leq \frac{1}{1 + e^{-(\max_{\mathbf{x}} \Delta \Delta G^{\circ}(\mathbf{x}, \mathbf{Y}^*, \mathbf{y}^*)) / RT}}. \quad (11)$$

As in the single-rival case, exhaustive enumeration over all sequences is unnecessary. Owing to the sparsity of loop energy contributions in the Turner model, it suffices to enumerate nucleotides on the *overall differential positions*

$$\Delta(Y_r, \mathbf{y}^*) = \cup_{\mathbf{y}' \in Y_r} \Delta(\mathbf{y}', \mathbf{y}^*). \quad (12)$$

Algorithm 2 outlines the resulting procedure for computing the upper bound using multiple rival structures.

3.3. Complexity Analysis

Algorithm 1 is a special case of Algorithm 2 with a single rival structure. The computational complexity of Algorithm 2 is determined by the size of the differential positions $\Delta(Y_r, y^*)$, as the algorithm enumerates all

Algorithm 2 Ensemble Approximation with Multiple Rival Structures (Motifs)

```

function ENSEMBLEAPPROXIMATION( $\mathbf{y}^*$ ,  $Y_r$ )
   $\Delta\Delta G_{max}^\circ \leftarrow -\infty$ 
  for  $\hat{\mathbf{x}} \in \{\mathbf{x} \vdash \Delta(Y_r, \mathbf{y}^*) \mid \mathbf{x} \in \mathcal{X}(\mathbf{y}^*)\}$  do
    if  $\Delta\Delta G^\circ(\hat{\mathbf{x}}, Y_r, \mathbf{y}^*) > \Delta\Delta G_{max}^\circ$  then
       $\Delta\Delta G_{max}^\circ = \Delta\Delta G^\circ(\hat{\mathbf{x}}, Y_r, \mathbf{y}^*)$ 
  return  $\frac{1}{1+e^{-\Delta\Delta G_{max}^\circ/RT}}$   $\triangleright$  upper bound  $pbound(\mathbf{y}^*)$ 

```

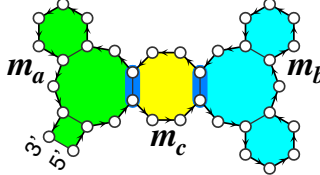


Fig. 4. Example of structure decomposition for the Eterna100 structure “multilooping fun”, which is decomposed into 3 motifs \mathbf{m}_a , \mathbf{m}_b , and \mathbf{m}_c highlighted in different colors.

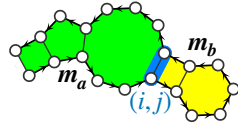


Fig. 5. A motif \mathbf{m} is split into \mathbf{m}_a and \mathbf{m}_b at the base pair (i, j)

nucleotide assignments restricted to these positions. Specifically, the time complexity is

$$O\left(6^{|pairs(\Delta(\mathbf{y}', \mathbf{y}^*))|} \cdot 4^{|unpaired(\Delta(\mathbf{y}', \mathbf{y}^*))|}\right), \quad (13)$$

where paired positions admit six canonical base-pair types and unpaired positions admit four nucleotides.

In practice, to control runtime, we sample rival structures (motifs) by folding sequences compatible with the target structure (motif) and impose an upper limit on the number of differential assignments enumerated. If this limit is exceeded and no suitable rival structures can be sampled, the corresponding structure or motif is skipped, trading completeness for efficiency.

4. Linear-time Dynamic Programming over Exponentially Many Decompositions

4.1. Structure and Probability Decomposition

FastMotif (Zhou *et al.*, 2025) shows that MFE-based structure undesignability can often be attributed to *local* (minimal) undesignable motifs. For example, Fig. 4 decomposes the Eterna100 structure *multilooping fun* into three motifs \mathbf{m}_a , \mathbf{m}_b , and \mathbf{m}_c ; in this instance, either \mathbf{m}_a or \mathbf{m}_b alone can certify the uMFE-undesignability of the full structure, providing a more localized and interpretable explanation than relying solely on global rival structures.

The principle that global designability is constrained by local designability also extends to *probabilistic* designability. CountingDesign (Yao, 2021) proved that for any motif \mathbf{m} contained in a target structure \mathbf{y}^* , the motif

probability upper-bounds the structure probability:

$$\forall \mathbf{m} \in \mathbf{y}^*, p(\mathbf{m} \mid \mathbf{x}) \leq p(\mathbf{y}^* \mid \mathbf{x}). \quad (14)$$

Applying this result to Fig. 4 yields, for example, $p(\mathbf{y}^* \mid \mathbf{x}) \leq p(\mathbf{m}_a \mid \mathbf{x})$ and $p(\mathbf{y}^* \mid \mathbf{x}) \leq p(\mathbf{m}_b \mid \mathbf{x})$.

However, CountingDesign relates $p(\mathbf{y}^* \mid \mathbf{x})$ to the probability of a *single* motif. The joint impact of multiple non-overlapping motifs remains unexplored. In this section, we show that when a structure can be decomposed into non-overlapping motifs, the structure probability is upper-bounded by the *product* of the motif probabilities.

Theorem 1 (Probability decomposition over non-overlapping motifs) *If a structure \mathbf{y}^* can be decomposed into a set of non-overlapping motifs $\mathcal{M} = \{\mathbf{m}_1, \mathbf{m}_2, \dots, \mathbf{m}_C\}$, then for any sequence $\mathbf{x} \in \mathcal{X}(\mathbf{y}^*)$,*

$$p(\mathbf{y}^* \mid \mathbf{x}) \leq \prod_{\mathbf{m} \in \mathcal{M}} p(\mathbf{m} \mid \mathbf{x}). \quad (15)$$

Proof As a structure can be decomposed recursively, it suffices to prove the binary splitting step. Suppose a motif \mathbf{m} is split into two submotifs \mathbf{m}_a and \mathbf{m}_b at a boundary base pair (i, j) , as illustrated in Fig. 5. Let $P_{i,j}$ denote the event that bases i and j are paired. By the chain rule of probability,

$$\begin{aligned}
 & p(\mathbf{m} \mid \mathbf{x}) \\
 &= p(\mathbf{m}_a + \mathbf{m}_b \mid \mathbf{x}) \\
 &= p(P_{i,j} \mid \mathbf{x}) \times p(\mathbf{m}_a \mid \mathbf{x}, P_{i,j}) \times p(\mathbf{m}_b \mid \mathbf{x}, P_{i,j}) \quad (16) \\
 &= p(P_{i,j} \mid \mathbf{x}) \times p(\mathbf{m}_a \mid \mathbf{x}) \times p(\mathbf{m}_b \mid \mathbf{x}) \\
 &\leq p(\mathbf{m}_a \mid \mathbf{x}) \times p(\mathbf{m}_b \mid \mathbf{x}).
 \end{aligned}$$

The third line holds because the conditioned boundary pair makes two motifs independent. The last line holds because once the boundary pairs are enforced at the motif-level RNA folding. \square

Corollary 1

$$pbound(\mathbf{y}^*) \leq \prod_{\mathbf{m} \in \mathcal{M}} pbound(\mathbf{m}). \quad (17)$$

This theorem suggests that we can tighten the probability upper bound for a structure by exploiting probability bounds of smaller local motifs. For sufficiently small motifs, we can obtain an exact bound by enumerating all compatible (partial) sequences and folding them under the motif constraints. For motifs that are too large for exhaustive enumeration, we instead apply the motif ensemble approximation with rival motifs developed in the previous section.

Figure 6 shows three alternative decompositions of the same Eterna100 structure from Fig. 4. In fact, a given target structure typically admits exponentially many decompositions, because each base pair may or may not be selected as a splitting boundary. This yields the following counting result.

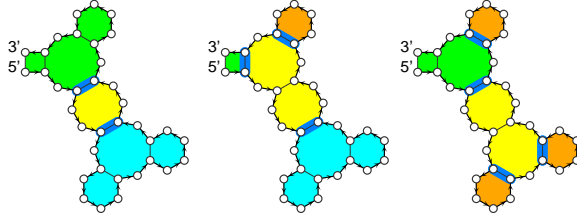


Fig. 6. Three different decompositions for the same structure shown in Fig. 4.

Theorem 2 *The total number of distinct decompositions of a secondary structure y is $2^{|pairs(y)|}$.*

Let \mathcal{M} denote the set of decompositions that can be evaluated efficiently for a target structure y^* . The best probability bound obtainable via decomposition is then

$$pbound(y^*) \leq \min_{M \in \mathcal{M}} \prod_{m \in M} pbound(m). \quad (18)$$

4.2. Optimal Decomposition Search by Linear-Time Dynamic Programming

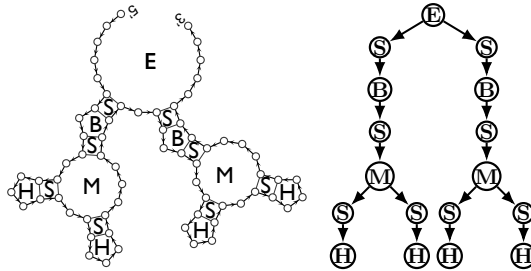


Fig. 7. Left: the Eterna100 structure *Chicken Feet*. Right: corresponding loop tree where each loop (including stacking) is represented as a node. E, S, B, H, M represent different loop types.

Although enumerating all decompositions is intractable, exploring more decompositions can only tighten the resulting upper bound. The key question is therefore how to search a large space of decompositions efficiently.

Inspired by dynamic programming techniques from compilers (Aho and Ullman, 1972; Aho and Johnson, 1976) and machine translation (Huang *et al.*, 2006), we propose a linear-time memoized top-down algorithm (Algorithm 3) that explores many decompositions while remaining computationally efficient. We represent a target structure by a fixed loop tree τ , where each

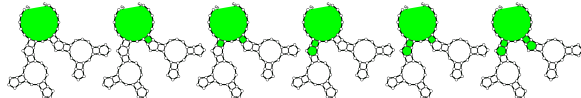


Fig. 8. Examples of motif candidates generated at the root node. For demonstration, here the maximum values for *depth*, *width*, and *number of loops* are set as 3, 2, and 5, respectively, and 6 out of 9 cases are shown. In experiments the maximum *depth* is set as 5.

Algorithm 3 Top-down Memoized Decomposition

```

1: function DECOMPOSE( $\eta$ )
2:   if  $cache[\eta]$  defined then
3:     return  $cache[\eta]$ 
4:    $best \leftarrow 1$ 
5:    $candidates \leftarrow \text{MOTIFGEN}(\eta, \text{depth}, \text{width}, \text{max\_loop})$ 
6:   for  $m_\eta \in candidates$  do  $\triangleright$  try each candidate  $m_\eta$ 
7:      $product \leftarrow pbound(m_\eta)$   $\triangleright$  exact or approx.
8:      $descendants \leftarrow \text{loop nodes adjacent to } m \text{ in } \tau_\eta$ 
9:     for  $\eta_i \in descendants$  do
10:       $(p_i, m_{\eta_i}^{\text{best}}) \leftarrow \text{DECOMPOSE}(\eta_i)$   $\triangleright$  recursion
11:       $product \leftarrow product \cdot p_i$ 
12:    if  $product < best$  then
13:       $best \leftarrow product$ 
14:       $m_\eta^{\text{best}} \leftarrow m_\eta$   $\triangleright$  plug in the results
15:     $cache[\eta] \leftarrow (best, m_\eta^{\text{best}})$   $\triangleright$  memoization
16:   return  $cache[\eta]$   $\triangleright$  optimal decomposition choice

```

node corresponds to a loop in the structure (Fig. 7). We decompose the structure by traversing τ top-down, starting at the root. When visiting a loop node η , we are solving the subproblem for the subtree τ_η , and we must choose a motif m_η that contains η . To avoid enumerating all possibilities, we constrain candidate motifs using three parameters: *depth*, *width*, and *number of loops*. Figure 8 shows examples of motif candidates generated when visiting the external loop at the root; the candidate-generation procedure is described in Algorithm 4. Once m_η is selected, we recursively process each adjacent descendant loop node η_i in the subtree τ_η . This procedure yields the following dynamic programming recurrence:

$$best(\tau_\eta) = \min_{m_\eta \in \text{MOTIFGEN}(\eta)} pbound(m_\eta) \prod_{\eta_i \in \text{descendants}(m_\eta)} best(\tau_{\eta_i}), \quad (19)$$

where $best(\tau_\eta)$ represents the tightest upper bound for the substructure rooted at the loop node η . The base case occurs when η is a hairpin loop, for which $best(\tau_\eta) = 1$.

Each loop node may admit many candidate motifs; the number of possible decompositions can also be calculated by dynamic programming recurrence:

$$count(\tau_\eta) = \sum_{m_\eta \in \text{MOTIFGEN}(\eta)} \prod_{\eta_i \in \text{descendants}(m_\eta)} count(\tau_{\eta_i}), \quad (20)$$

with the base case value of 1. As a result, the decomposition possibilities grows exponentially with the size of the loop tree and We address this via memoization: each subtree rooted at a loop node is solved at most once and cached. We also store backpointers to recover the best motif choice at each node, and reconstruct the optimal decomposition by backtracking. The resulting dynamic program runs in $O(\alpha\beta)$ time, where α is the number of loop nodes in the loop tree and β is the maximum number of motif candidates considered at any node.

Algorithm 4 Constrained Motif Generation from a Loop

```

1: function MOTIFGEN( $\eta$ , max_depth, max_width, max_loop)
2:   candidates  $\leftarrow \emptyset$ 
3:   for  $d \leftarrow 1$  to max_depth do
4:      $M_d \leftarrow \emptyset$   $\triangleright$  motifs of depth  $d$  to be generated
5:     if  $d = 1$  then
6:        $M_d \leftarrow \{\eta\}$   $\triangleright$  the motif is a single node  $\eta$ 
7:     else
8:       for  $m \in M_{d-1}$  do
9:          $m_{\text{new}} \leftarrow \text{GROW}(m)$ 
10:        if  $\text{WIDTH}(m_{\text{new}}) > \text{max\_width}$  then
11:          continue
12:        if  $|\text{LOOPS}(m_{\text{new}})| > \text{max\_loop}$  then
13:          continue
14:         $M_d \leftarrow M_d \cup m_{\text{new}}$ 
15:        candidates  $\leftarrow i\text{candidates} \cup M_d$ 
16:   return candidates

```

5. Experiments

5.1. Settings

5.1.1. Implementation

We call our method *LinearDecomposition*, which consists of two core components: (i) Linear-Time Dynamic Decomposition (Algorithm 3) and (ii) Ensemble Approximation (Algorithm 2).

The dynamic decomposition module efficiently searches for the optimal motif decomposition by the recurrence formula Eq. 19 over exponentially many candidates. The ensemble approximation module estimates probability bounds $p\text{bound}(\mathbf{y}^*)$ or $p\text{bound}(\mathbf{m}^*)$ for a target structure or motif.

All experiments use ViennaRNA (v2.7) folding energy parameters (Lorenz *et al.*, 2011). Algorithms are implemented in C++ on Linux machines with 4.0 GHz CPUs and 32 GB memory. Ensemble approximation is parallelized with OpenMP over 90 CPU cores.

During decomposition search, Algorithm 3 repeatedly queries motif probability bounds $p\text{bound}(\mathbf{m}_\eta)$ (line 7). To improve efficiency, we precompute and cache motif bounds using a hybrid strategy: (1) exact bounds via exhaustive enumeration for motifs of length ≤ 14 , following CountingDesign (Yao, 2021); and (2) non-exact bounds via ensemble approximation for larger motifs.

5.1.2. Datasets

We evaluate our method, *LinearDecomposition*, on two widely used RNA structure benchmarks.

1. **ArchiveII100.** ArchiveII (Sloma and Mathews, 2016; Cannone *et al.*, 2002) contains native RNA secondary structures spanning 10 families of naturally occurring RNAs, including tRNA, rRNA, etc. We remove pseudoknotted structures and those incompatible with ViennaRNA’s default loop constraints. We retain structures of length > 200 , resulting in 1,144 structures.
2. **Eterna100.** Eterna100 (Anderson-Lee *et al.*, 2016) consists of 100 secondary structures designed by

human players of Eterna and is widely used for evaluating RNA design and designability.

We compare against CountingDesign and an enhanced variant: We compare against CountingDesign and an enhanced variant:

1. **CountingDesign.** CountingDesign (Yao *et al.*, 2019; Yao, 2021) can identify exact probability bounds for short motifs (up to length 14) by exhaustively enumerating RNA sequences for each motif. However, the method is not scalable and lacks explainability.
2. **CountingDesign+.** We extend CountingDesign to include motifs with external loops, aligning its motif definition with ours, since its motif definition is narrower than ours.

5.2. Overall Results

Table 1. Average probability bounds on each benchmark.

| Benchmarks | ArchiveII | Eterna100 |
|---|--------------|--------------|
| Number of distinct structures (\mathbf{y}^*) | 1144 | 100 |
| $p(\mathbf{y}^* \mathbf{x})$, Achieved by RNA Design | 0.766 | 0.599 |
| $p\text{bound}(\mathbf{y}^*)$, CountingDesign | 0.898 | 0.896 |
| $p\text{bound}(\mathbf{y}^*)$, CountingDesign+ | 0.875 | 0.876 |
| $p\text{bound}(\mathbf{y}^*)$, LinearDecomposition | 0.800 | 0.741 |

Table 1 reports average probability bounds on both datasets. For reference, we also include the highest structure probabilities achieved by RNA design methods such as SAMFEO (Zhou *et al.*, 2023) and SamplingDesign (Tang *et al.*, 2025).

LinearDecomposition consistently yields the tightest bounds, improving over CountingDesign+ by 0.075 on ArchiveII and 0.135 on Eterna100. This improvement is expected, as *LinearDecomposition* is theoretically guaranteed to produce bounds no worse than CountingDesign.

We also observe a clear correlation between probability bounds and empirical designability. ArchiveII structures are generally more designable: the average bound (0.800) is close to the achieved probability (0.766). In contrast, Eterna100 structures are less designable, with a larger gap between the achieved probability (0.599) and the bound (0.741).

5.3. Detailed Results

Figures 9 and 10 show per-structure bounds and achieved probabilities. Bounds tend to be tighter for both highly designable and highly undesignable structures. Highly designable structures typically consist of motifs with uniformly high local probabilities, while highly undesignable structures often contain multiple motifs with very low bounds, sometimes leading to near-zero global bounds.

These bounds also provide a useful lens for evaluating RNA design results. For example, a structure achieving probability 0.7 may be closer to its theoretical limit than another achieving 0.8 if its bound is substantially lower.

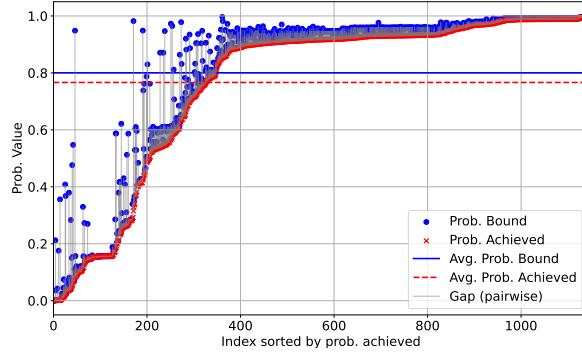


Fig. 9. Probability bounds vs. achieved probabilities on ArchiveII.

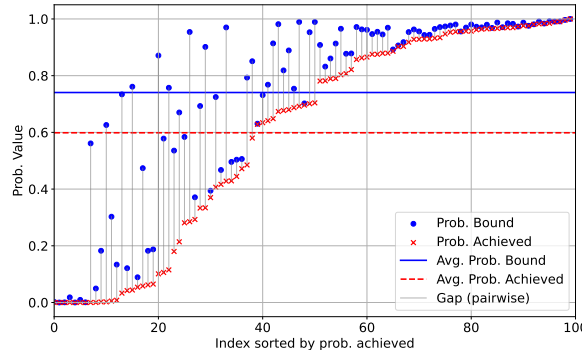


Fig. 10. Probability bounds vs. achieved probabilities on Eterna100.

5.4. Ablation Study

To assess the two core components of LINEARDECOMPOSITION, we perform two ablations: (1) disable motif ensemble approximation by setting approximate motif bounds to 1; and (2) disable dynamic decomposition by using only the minimum single-motif bound.

Table 2. Ablation study results.

| Benchmarks | ArchiveII | Eterna100 |
|----------------------------------|--------------|--------------|
| LinearDecomposition | 0.800 | 0.741 |
| w/o motif ensemble approximation | 0.866 | 0.839 |
| w/o dynamic decomposition | 0.819 | 0.787 |

As shown in Table 2, both ablations lead to looser bounds, confirming the importance of both components. Nevertheless, the ablated variants still outperform the baselines in Table 1, demonstrating the robustness of the framework.

5.5. Designability Dissection

Table 3 presents a structural dissection of several Eterna100 puzzles previously shown to be uMFE-undesignable (Zhou et al., 2025). For each structure y^* , we report the total number of decompositions (via dynamic programming Eq. 20) explored by LinearDecomposition,

the optimal decomposition achieving the tightest probability bound, and the resulting global probability upper bound $pbound(y^*)$.

Despite the large number of possible decompositions, ranging from hundreds to millions, LinearDecomposition consistently identifies a small set of local motifs whose combined bounds dominate the global probability bound. Notably, structures with complex multiloop or bulge configurations (e.g., *multilooping fun*) exhibit extremely low bounds, indicating that probabilistic undesignability can often be traced to a few highly constraining motifs. These results highlight the value of decomposition-based analysis for pinpointing the structural origins of low RNA designability.

Table 3. Structure Dissection with Eterna100 Puzzles.

| Puzzle (y^*) | Decomposition #of explored | Optimal | $pbound(y^*)$ |
|----------------------|-------------------------------|---------|---------------|
| 1, 2, 3 and 4 bulges | 2,734,333 | | 0.3026 |
| Repetit. Seqs. 8/10 | 860 | | 0.1874 |
| multilooping fun | 119 | | 0.0006 |
| Chicken feet | 52,114 | | 0.1336 |

5.6. Efficiency

The runtime of LinearDecomposition consists of decomposition search and motif ensemble approximation. Decomposition search is fast, averaging 0.01 s per structure on ArchiveII and 0.9 s on Eterna100. Ensemble approximation estimates bounds for 15,000 and 9,700 unique motifs on ArchiveII and Eterna100, with an average cost of 7.6 s and 10.7 s per motif, respectively. The total time cost average per structure is 106 seconds and 1039 seconds on ArchiveII and Eterna100, respectively. Importantly, each motif bound is computed only once and cached. As a result, the amortized runtime of LinearDecomposition is under 1 s per structure on both datasets.

6. Discussion and Conclusion

We introduced a theoretical framework based on ensemble approximation and probability decomposition to quantify the probabilistic designability of RNA secondary structures under the nearest-neighbor model. We further develop a linear-time dynamic-programming algorithm that efficiently searches for optimal decompositions among exponentially many candidates. Together, the resulting bounds and accompanying theorems provide

mechanistic insights into why certain RNA structures exhibit intrinsically low probabilistic designability.

Applied to the ArchiveII and Eterna100 datasets, our algorithm LINEARDECOMPOSITION consistently produces tighter probability bounds under the Turner energy model than existing methods. Moreover, the resulting optimal decompositions offer interpretable explanations of structural design difficulty by identifying the specific motifs that limit global designability.

Despite these strengths, LINEARDECOMPOSITION has several limitations:

1. Unless a structure is designed with a probability close to the probability bound found by LinearDecomposition, the bound may be optimistic, thus loose.
2. Ensemble approximation is not universally applicable; for some structures or motifs, suitable rival motifs are hard to sample.

Future work includes improving rival motif generation to tighten ensemble approximations and leveraging the optimal decomposition given by LINEARDECOMPOSITION as a guide for RNA design.

References

Aguirre-Hernández, R., Hoos, H. H. and Condon, A. (2007). Computational RNA secondary structure design: empirical complexity and improved methods. *BMC bioinformatics*, **8**(1), 1–16.

Aho, A. V. Johnson, S. C. (1976). Optimal code generation for expression trees. *Journal of the ACM (JACM)*, **23**(3), 488–501.

Aho, A. V. Ullman, J. D. (1972). *The theory of parsing, translation, and compiling*, volume 1. Prentice-Hall Englewood Cliffs, NJ.

Anderson-Lee, J., Fisker, E., Kosaraju, V., Wu, M., Kong, J., Lee, J., Lee, M., Zada, M., Treuille, A. and Das, R. (2016). Principles for predicting RNA secondary structure design difficulty. *Journal of molecular biology*, **428**(5), 748–757.

Cannone, J. J., Subramanian, S., Schnare, M. N., Collett, J. R., D’Souza, L. M., Du, Y., Feng, B., Lin, N., Madabusi, L. V., Müller, K. M., Pande, N., Shang, Z., Yu, N. and Gutell, R. R. (2002). The Comparative RNA Web (CRW) Site: An Online Database of Comparative Sequence and Structure Information for Ribosomal, Intron, and Other RNAs. *BioMed Central Bioinformatics*, **3**(2).

Coller, J. Ignatova, Z. (2024). tRNA therapeutics for genetic diseases. *Nature Reviews Drug Discovery*, **23**(2), 108–125.

Doudna, J. A. Cech, T. R. (2002). The chemical repertoire of natural ribozymes. *Nature*, **418**(6894), 222–228.

Haleš, J., Maňuch, J., Ponty, Y. and Stacho, L. (2015). Combinatorial RNA design: designability and structure-approximating algorithm. In *Combinatorial Pattern Matching: 26th Annual Symposium, CPM 2015, Ischia Island, Italy, June 29–July 1, 2015, Proceedings*, pages 231–246. Springer.

Huang, L., Knight, K. and Joshi, A. (2006). Statistical syntax-directed translation with extended domain of locality. In *Proceedings of the 7th Conference of the Association for Machine Translation in the Americas: Technical Papers*, pages 66–73.

Lorenz, R., Bernhart, S. H., Zu Siederdissen, C. H., Tafer, H., Flamm, C., Stadler, P. F. and Hofacker, I. L. (2011). ViennaRNA Package 2.0. *Algorithms for Molecular Biology*, **6**(1), 1.

Mathews, D. H. Turner, D. H. (2006). Prediction of RNA secondary structure by free energy minimization. *Current Opinion in Structural Biology*, **16**(3), 270–278.

Mathews, D. H., Disney, M. D., Childs, J. L., Schroeder, S. J., Zuker, M. and Turner, D. H. (2004). Incorporating chemical modification constraints into a dynamic programming algorithm for prediction of RNA secondary structure. *Proceedings of the National Academy of Sciences U.S.A.*, **101**(19), 7287–7292.

Portela, F. (2018). An unexpectedly effective Monte Carlo technique for the RNA inverse folding problem. *BioRxiv*, page 345587.

Sloma, M. Mathews, D. (2016). Exact calculation of loop formation probability identifies folding motifs in RNA secondary structures. *RNA*, **22**, 1808–1818.

Tang, W. Y., Dai, N., Zhou, T., Mathews, D. and Huang, L. (2025). Samplingdesign: Rna design via continuous optimization with coupled variables and monte-carlo sampling.

Turner, D. H. Mathews, D. H. (2010). NNDB: the nearest neighbor parameter database for predicting stability of nucleic acid secondary structure. *Nucleic Acids Research*, **38**(suppl_1), D280–D282.

Ward, M., Courtney, E. and Rivas, E. (2023). Fitness functions for rna structure design. *Nucleic Acids Research*, **51**(7), e40–e40.

Yao, H.-T. (2021). *Local decomposition in RNA structural design*. Ph.D. thesis, McGill University (Canada).

Yao, H.-T., Chauve, C., Regnier, M. and Ponty, Y. (2019). Exponentially few RNA structures are designable. In *Proceedings of the 10th ACM International Conference on Bioinformatics, Computational Biology and Health Informatics*, pages 289–298.

Zhou, T., Dai, N., Li, S., Ward, M., Mathews, D. H. and Huang, L. (2023). RNA design via structure-aware multifrontier ensemble optimization. *Bioinformatics*, **39**(Supplement_1), i563–i571.

Zhou, T., Tang, W. Y., Mathews, D. H. and Huang, L. (2024). Undesignable rna structure identification via rival structure generation and structure decomposition. In *International Conference on Research in Computational Molecular Biology*, pages 270–287. Springer.

Zhou, T., Malik, A., Tang, W. Y., Mathews, D. H. and Huang, L. (2025). Scalable and interpretable identification of minimal undesignable rna structure motifs with rotational invariance. In *International Conference on Research in Computational Molecular Biology*, pages 153–174. Springer.

Supplementary Information

S1. Structural Loops

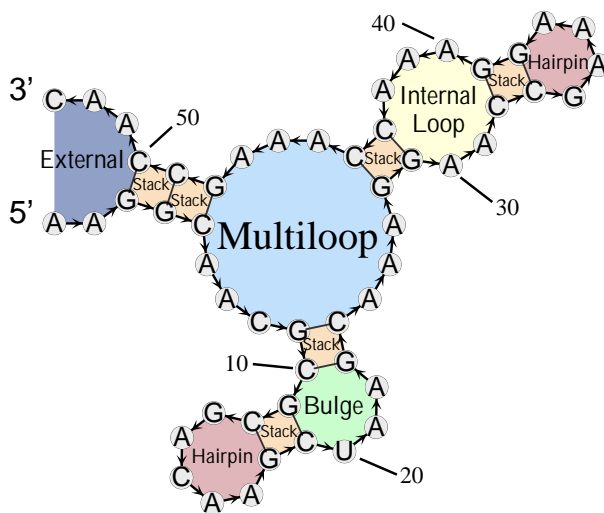


Fig. S1. An example of secondary structure and loops.

A secondary secondary structure can be decomposed into a collection of loops, where each loop is usually a region enclosed by base pair(s). Depending on the number of pairs on the boundary, main types of loops include hairpin loop, internal loop and multiloop, which are bounded by 1, 2 and 3 or more base pairs, respectively. In particular, the external loop is the most outside loop and is bounded by two ends (5' and 3') and other base pair(s). Thus each loop can be identified by a set of pairs. Fig. S1 showcases an example of secondary structure with various types of loops, where the some of the loops are notated as

1. Hairpin: $H\langle(12, 18)\rangle$.
2. Bulge: $B\langle(10, 23), (11, 19)\rangle$.
3. Stack: $S\langle(3, 50), (4, 49)\rangle$.
4. Internal Loop: $I\langle(29, 43), (32, 39)\rangle$.
5. Multiloop: $M\langle(5, 48), (9, 24), (28, 44)\rangle$.
6. External Loop: $E\langle(3, 50)\rangle$.

Table S1. Critical positions of loops in Fig. 1

| Loop Type | Critical Positions | |
|-----------|----------------------------|-----------------------|
| | Closing Pairs | Mismatches (Unpaired) |
| External | (3, 50) | 2, 51 |
| Stack | (3, 50), (4, 49) | |
| Stack | (4, 49), (5, 48) | |
| Multi | (5, 48), (9, 24), (28, 44) | 4, 49, 8, 25, 27, 45 |
| Stack | (9, 24), (10, 23) | |
| Bulge | (10, 23), (11, 19) | |
| Stack | (11, 19), (12, 18) | |
| Hairpin | (12, 18) | 13, 17 |
| Stack | (28, 44), (29, 43) | |
| Internal | (29, 43), (32, 39) | 30, 42, 31, 40 |
| Stack | (32, 39), (33, 38) | |
| Hairpin | (33, 38) | 34, 37 |

The function $loops(\mathbf{y})$ is used to denote the set of loops in a structure \mathbf{y} . The free energy of a secondary structure \mathbf{y} is the sum of the free energy of each loop,

$$\Delta G^\circ(\mathbf{x}, \mathbf{y}) = \sum_{\mathbf{z} \in loops(\mathbf{y})} \Delta G^\circ(\mathbf{x}, \mathbf{z}),$$

The energy of each loop is typically determined by nucleotides on the positions of enclosing pairs and their adjacent mismatch positions, which are named as *critical positions* in this article. Table S1 lists the critical positions for all the loops in Fig. 1 and Table S2 shows the indices of critical positions for each type of loops. Additionally, some special hairpins of unstable triloops and stable tetraloops and hexaloops in Turner model have a separate energy lookup table. When evaluating the energy of a loop, it suffices to input only the nucleotides on its critical positions, i.e.,

$$\Delta G^\circ(\mathbf{x}, \mathbf{y}) = \sum_{\mathbf{z} \in loops(\mathbf{y})} \Delta G^\circ(\mathbf{x} \vdash critical(\mathbf{z}), \mathbf{z}), \quad (21)$$

where $critical(\mathbf{z})$ denotes the critical positions of loop \mathbf{z} and $\mathbf{x} \vdash critical(\mathbf{z})$ denotes the nucleotides from \mathbf{x} that are “projected” onto $critical(\mathbf{z})$. The projection (\vdash) allows us to focus on the relevant nucleotides for energy evaluation. For instance,

$$critical(H\langle(12, 18)\rangle) = \{12, 13, 17, 18\}, \quad (22)$$

$$critical(I\langle(29, 43), (32, 39)\rangle) = \{29, 30, 31, 32, 39, 40, 42, 43\}. \quad (23)$$

For convenience, we also interchangeably put paired positions in brackets, i.e.,

$$critical(H\langle(12, 18)\rangle) = \{(12, 18), 13, 17\}, \quad (24)$$

$$critical(I\langle(29, 43), (32, 39)\rangle) = \{(29, 43), (32, 39), 30, 31, 40, 42\}. \quad (25)$$

Table S2. Critical positions for each type of loops under the Turner model implemented in ViennaRNA. Special hairpins (Mathews *et al.*, 2004) (triloops, tetraloops, and hexaloops) are not considered.

| Loop Type | Critical Positions | |
|------------------|---|---|
| | Closing Pairs | Mismatches |
| External Hairpin | $(i_1, j_1), (i_2, j_2), \dots, (i_k, j_k)$ (i, j) | $(i_1 - 1, j_1 + 1), \dots, (i_k - 1, j_k + 1)$ $i + 1, j - 1$ |
| Stack | $(i, j), (k, l)$ | — |
| Bulge | $(i, j), (k, l)$ | — |
| Internal | $(i, j), (k, l)$ | $i + 1, j - 1, k - 1, l + 1$ |
| Multi | $(i, j), (i_1, j_1), \dots, (i_k, j_k)$ | $i + 1, j - 1, \dots, i_k - 1, j_k + 1$ |

S2. Structural Motif

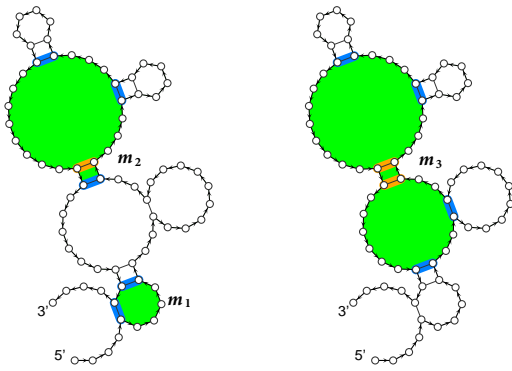


Fig. S2. Motifs of various cardinalities (numbers of loops): $card(\mathbf{m}_1) = 1$, $card(\mathbf{m}_2) = 2$, $card(\mathbf{m}_3) = 3$. Loops are highlighted in green, internal pairs ($ipairs$) in orange and boundary pairs ($bpairs$) in blue.

S2.1. Motif is a Generalization of Structure

Definition 1 A motif \mathbf{m} is a contiguous (sub)set of loops in an RNA secondary structure \mathbf{y} , notated $\mathbf{m} \subseteq \mathbf{y}$.

Many functions defined for secondary structures can also be applied to motifs. For example, $loops(\mathbf{m})$ represents the set of loops within a motif \mathbf{m} , while $pairs(\mathbf{m})$ and $unpaired(\mathbf{m})$ represent the sets of base pairs and unpaired positions, respectively. We define the *cardinality* of \mathbf{m} as the number of loops in \mathbf{m} , i.e., $card(\mathbf{m}) = |loops(\mathbf{m})|$. Fig. S2 illustrates three motifs, \mathbf{m}_1 , \mathbf{m}_2 , and \mathbf{m}_3 , in a structure adapted from the Eterna puzzle “Cat’s Toy”. These motifs contain 1, 2, and 3 loops, respectively. We also define the *length* of a motif $|\mathbf{m}|$ as the number of bases it contains, which is consistent with the length of a secondary structure $|\mathbf{y}|$.

Since motifs are defined as sets of loops, we can conveniently use set relations to describe their interactions. A motif \mathbf{m}_A is a *sub-motif* of another motif \mathbf{m}_B if \mathbf{m}_A is contained within \mathbf{m}_B , denoted as $\mathbf{m}_A \subseteq \mathbf{m}_B$. For the motifs in Fig. S2, we observe the relation $\mathbf{m}_2 \subseteq \mathbf{m}_3$. We further use $\mathbf{m}_A \subset \mathbf{m}_B$ to indicate that \mathbf{m}_A is a

proper sub-motif of \mathbf{m}_B , meaning $\mathbf{m}_A \neq \mathbf{m}_B$. Therefore, $\mathbf{m}_2 \subset \mathbf{m}_3$. The entire structure \mathbf{y} can be regarded as the largest motif within itself, and accordingly, $\mathbf{m} \subseteq \mathbf{y}$ signifies that motif \mathbf{m} is a part of structure \mathbf{y} , with $\mathbf{m} \subset \mathbf{y}$ implying \mathbf{m} is strictly smaller than \mathbf{y} .

The loops in a motif \mathbf{m} are connected by base pairs. Each base pair in $pairs(\mathbf{m})$ is classified as either an *internal pair* linking two loops in \mathbf{m} or a *boundary pair* connecting one loop inside \mathbf{m} to one outside. These two types of pairs in \mathbf{m} are denoted as disjoint sets $ipairs(\mathbf{m})$ and $bpairs(\mathbf{m})$, respectively:

$$ipairs(\mathbf{m}) \cap bpairs(\mathbf{m}) = \emptyset, \quad ipairs(\mathbf{m}) \cup bpairs(\mathbf{m}) = pairs(\mathbf{m}). \quad (26)$$

Utilizing the commonly accepted nearest neighbor model for RNA folding, it becomes evident that certain motifs may be absent from structures folded from RNA sequences. For instance, motif \mathbf{m}_3 in Fig. S2 is considered undesignable, as the removal of its two internal pairs consistently reduces the free energy. This brings us to the definition of an *undesignable motif*.

S2.2. Motif Ensemble from Constrained Folding

The designability of motifs is based on *constrained folding*. Given a sequence \mathbf{x} , a structure in its ensemble $\mathbf{y} \in \mathcal{Y}(\mathbf{x})$, we can conduct constrained folding by constraining the boundary pairs of \mathbf{m} , i.e., $bpairs(\mathbf{m})$. We generalize the concept of (structure) *ensemble* to *motif ensemble* as the set of motifs that \mathbf{x} can possibly fold into (under the constraint $bpairs(\mathbf{m})$ being forced), denoted as $\mathcal{M}(\mathbf{x}, bpairs(\mathbf{m}))$. In the context of constrained folding, the folding outcomes are unaffected by the nucleotides at the constrained positions. Thus, with slight notation abuse, we use \mathbf{x} to denote a partial sequence corresponding to a motif \mathbf{m} , where each position in \mathbf{x} matches a position in \mathbf{m} , and vice versa. By this definition, the motif ensemble of a partial sequence \mathbf{x} is denoted as $\mathcal{M}(\mathbf{x})$. Similarly, the notation $\mathcal{X}(\mathbf{m})$ generalizes $\mathcal{X}(\mathbf{y})$ and represents all (partial) RNA sequences whose motif ensembles contain \mathbf{m} . Motifs in $\mathcal{M}(\mathbf{x}, bpairs(\mathbf{m}))$ have the same boundary pairs, i.e.,

$$\forall \mathbf{m}', \mathbf{m}'' \in \mathcal{M}(\mathbf{x}), \quad bpairs(\mathbf{m}') = bpairs(\mathbf{m}'') = bpairs(\mathbf{m}). \quad (27)$$

The *free energy change* of a motif \mathbf{m} is the sum of the free energy of the loops in \mathbf{m} ,

$$\Delta G^\circ(\mathbf{x}, \mathbf{m}) = \sum_{\mathbf{z} \in \text{loops}(\mathbf{m})} \Delta G^\circ(\mathbf{x}, \mathbf{z}). \quad (28)$$

The definitions of MFE and uMFE can also be generalized to motifs via constrained folding.

Definition 2 A motif $\mathbf{m}^* \subseteq \mathbf{y}$ is an MFE motif of folding \mathbf{x} under constraint $\text{bpairs}(\mathbf{m})$, i.e., $\text{MFE}(\mathbf{x}, \text{bpairs}(\mathbf{m}))$, if and only if

$$\forall \mathbf{m} \in \mathcal{M}(\mathbf{x}, \text{bpairs}(\mathbf{m})) \text{ and } \mathbf{m} \neq \mathbf{m}^*, \Delta G^\circ(\mathbf{x}, \mathbf{m}^*) \leq \Delta G^\circ(\mathbf{x}, \mathbf{m}). \quad (29)$$

Definition 3 A motif $\mathbf{m}^* \subseteq \mathbf{y}$ is an uMFE motif of folding \mathbf{x} under constraint $\text{bpairs}(\mathbf{m})$, i.e., $\text{uMFE}(\mathbf{x}, \text{bpairs}(\mathbf{m}))$, if and only if

$$\forall \mathbf{m} \in \mathcal{M}(\mathbf{x}, \text{bpairs}(\mathbf{m})) \text{ and } \mathbf{m} \neq \mathbf{m}^*, \Delta G^\circ(\mathbf{x}, \mathbf{m}^*) < \Delta G^\circ(\mathbf{x}, \mathbf{m}). \quad (30)$$

Similarly, the equilibrium probability of a sequence folding into the motif is defined as,

$$p(\mathbf{m} \mid \mathbf{x}) = \frac{e^{-\Delta G^\circ(\mathbf{x}, \mathbf{m})/RT}}{Q(\mathbf{x})} = \frac{e^{-\Delta G^\circ(\mathbf{x}, \mathbf{m})/RT}}{\sum_{\mathbf{m}' \in \mathcal{M}(\mathbf{x}, \text{bpairs}(\mathbf{m}))} e^{-\Delta G^\circ(\mathbf{x}, \mathbf{m}')/RT}}. \quad (31)$$